Analysis of the numerical properties of the transmission line matrix model for outdoor sound propagation

Quentin Goestchel, Gwenaël Guillaume, David Ecotière, Benoit Gauvreau

Analysis of the numerical properties of the transmission line matrix model for outdoor sound propagation

Quentin Goestchel[a], Gwenaël Guillaume[a,*], David Ecotière[a], Benoit Gauvreau[b]

[a] *UMRAE, CEREMA, Univ Gustave Eiffel, IFSTTAR, F-67035 Strasbourg, France*
[b] *UMRAE, Univ Gustave Eiffel, IFSTTAR, CEREMA, F-44344 Bouguenais, France*

Abstract

Outdoor sound propagation modeling can be performed through various numerical models. Nowadays, time-domain methods are widely used and enable accurate simulations for most of the sound physical phenomena involved in environmental acoustics. However, the transmission line matrix (TLM) method remains relatively poorly documented. In this paper, a thorough review of the method and a stability analysis are provided. The review of the model leads to a more robust understanding of its link with the wave equation using Taylor expansions. Two different cases are considered: a homogeneous non-dissipative medium and an inhomogeneous dissipative one. The stability analysis shows the quantification of the model inherent dispersion error and highlights similarities with a finite difference scheme. To conclude, a numerical experiment aims to characterize precisely the limitations of the method applied to outdoor sound propagation.

Keywords: Transmission Line Matrix Method, Numerical Methods, Outdoor Sound Propagation, Dispersion

1. Introduction

Anthropogenic noise pollution is known to have a negative impact on public health and on biodiversity [1–3]. Disturbing sounds generated by human activities are not confined to urban environments and reach further into natural areas. Predictions of long-range outdoor sound propagation are useful for assessing the impact of noise pollution on living beings and their environment. For this purpose, numerical acoustic models are necessary and a large number of them are available in the literature [4, 5]. From frequency domain methods to time domain methods, the study and improvement of these models have recently developed with the available computing power.

*Corresponding author
Email address: gwenael.guillaume@cerema.fr (Gwenaël Guillaume)

Unlike other time-domain numerical methods such as finite differences or the Fourier pseudospectral time-domain method, the transmission line matrix method (TLM) has not been documented extensively [5–7]. Originally introduced to model high frequency electromagnetic fields, the TLM model and its formalism were introduced in 1971 [8, 9]. In his book, de Cogan showed the flexibility of this method by applying it to various domains and for electromagnetic waves, the TLM model seems to tackle with most of the difficulties usually encountered by numerical methods such as perfectly matched layers (PML), moving boundaries, or non-cartesian meshes [10, 11].

In the field of acoustics, the TLM model is successfully used in room acoustics and the essence of the method has been studied from a theoretical point of view [12, 13]. For outdoor scenarios, application to inhomogeneous media, urban areas or even forest-like environments have been developed and compared to experimental results [14–16]. The numerical scheme has even been optimized by making it capable of running on parallel graphic processing units [17]. Finally, complex features such as impedance boundary conditions or meteorological effects have been introduced into the TLM model in order to model more realistic environments [11, 18].

However, no stability analysis of the method has been undertaken yet. Therefore, this paper aims to quantitatively define the limitations of the TLM method through an extensive theoretical analysis. The scope of the study focuses on long-range outdoor noise predictions, as they are complex situations to model and therefore the most likely to expose limitations of numerical models. For this purpose, only the central scheme is considered, leaving aside boundary conditions, PMLs and other artifacts inducing numerical errors.

An updated theoretical d-dimension formalism of the TLM is first proposed in the next section. In the third and fourth section, the model is detailed for a homogeneous non-dissipative and an inhomogeneous dissipative case, respectively. Within each part, the link with the wave equation is demonstrated and a stability analysis is performed, highlighting the inherent dispersion error of the model. In a last section, a numerical experiment is presented and an analysis of the results is given and interpreted in order to summarize precisely the limitations of the TLM model use for outdoor sound propagation.

2. Theoretical basis

2.1. Overall formalism

Unlike most numerical methods, the TLM is not initially derived from the conservative first order equations. It is based on the Huygens' principle for wave propagation and on an electro-acoustical analogy [12]. The property of a wavefront to be recursively discretized in the form of punctual secondary sources is exploited and applied to a Cartesian mesh. The sound propagation is then modeled as pressure pulses, propagating along transmission lines. This decomposition of the propagation mechanism is the TLM basis. It allows the analogy between the progression of a sound wave and the diffusion of pulses between the nodes of a mesh.

In the following, a d-dimension spatial generalization inspired from previous works is described [19]. The spatial domain is equally discretized in every directions with steps $\Delta\ell$ such as $x_d = j_d\Delta\ell,\ j_d \in \mathbb{Z}$ and the time is decomposed into steps such as $t_n = n\Delta t,\ n \in \mathbb{N}$. The spatial locations of nodes on the grid are then represented by the vector of indices: $\mathbf{r} = (j_1, \ldots, j_d)$. The core of the model is that each node in the volume under consideration receives and emits incident and scattered pulses instantaneously, at each time step n. These pressure pulses are travelling along links between the nodes, named transmission lines m. The formalism for this representation is given as follow: ${}_nI^m_{\mathbf{r}}$ is the incident pressure pulse to the node $\mathbf{r}$ along the line m at the time step n and ${}_nS^m_{\mathbf{r}}$ is the reflected instantaneous scattered pulse.

2.2. Scattering matrix

Expressing this mechanism in d-dimensions leads to the main asset of the TLM method: the scattered pulses are calculated only with the matrix relation:

$$ {}_n\underline{\mathrm{S}}_{\mathbf{r}} = {}_n\underline{\underline{D}}_{\mathbf{r}} \cdot {}_n\underline{\mathrm{I}}_{\mathbf{r}}, \tag{1} $$

with ${}_n\underline{\mathrm{S}}_{\mathbf{r}}$ and ${}_n\underline{\mathrm{I}}_{\mathbf{r}}$ the scattered and incident pulses vectors and ${}_n\underline{\underline{D}}_{\mathbf{r}}$ the diffusion matrix

$$ {}_n\underline{\underline{D}}_{\mathbf{r}} = {}_n\begin{bmatrix} R^1_{\mathbf{r}} & T^2_{\mathbf{r}} & \cdots & \cdots & T^M_{\mathbf{r}} \\ T^1_{\mathbf{r}} & R^2_{\mathbf{r}} & T^m_{\mathbf{r}} & \cdots & \vdots \\ \vdots & T^2_{\mathbf{r}} & \ddots & T^m_{\mathbf{r}} & \vdots \\ \vdots & \vdots & T^m_{\mathbf{r}} & R^m_{\mathbf{r}} & T^M_{\mathbf{r}} \\ T^1_{\mathbf{r}} & \cdots & \cdots & T^m_{\mathbf{r}} & R^M_{\mathbf{r}} \end{bmatrix}_{\mathbf{r}}, \tag{2} $$

with $m \in M$, the number of lines around a node. The $M \times M$ matrix is populated with the pressure reflection and transmission coefficients, representing the behavior of pressures pulses encountering impedance discontinuities at a node, leading to reflections in the incident transmission lines and "scattering" in the others, whose impedance coefficients are formulated as $Z^m_{L_{\mathbf{r}}}$. $Z^m_{T_{\mathbf{r}}}$ is the impedance of the equivalent medium after the node discontinuity, as illustrated by Fig. 1(a). Fig. 1 represents these mechanisms in the 2D case of an incident pulse to a node from a single transmission line. The general expressions of the coefficients are:

$$ R^m_{\mathbf{r}} = \frac{Z^m_{T_{\mathbf{r}}} - Z^m_{L_{\mathbf{r}}}}{Z^m_{T_{\mathbf{r}}} + Z^m_{L_{\mathbf{r}}}}, \tag{3a} $$

$$ T^m_{\mathbf{r}} = 1 + R^m_{\mathbf{r}}. \tag{3b} $$

2.3. Connection laws

To complete the method, connection laws, describing the time relation between the scattered pulses at t_n and incident pulses at t_{n+1} are needed. A

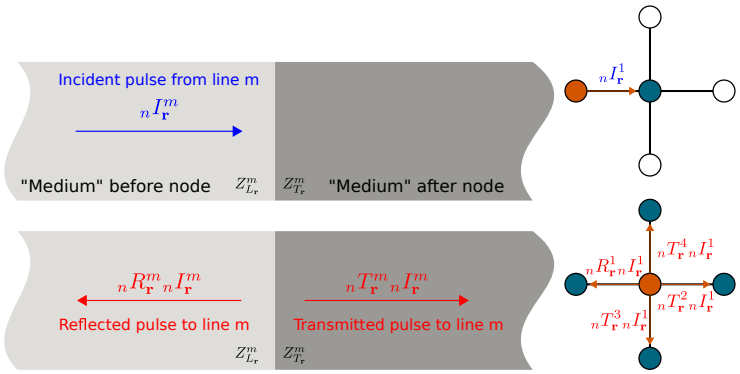

Figure 1: Phenomenological representation of an incident pulse reaching a node: (a) as a medium discontinuity, (b) on a 2D grid. The convention adopted for the lines numerotation is from left to right and from bottom to top.

d-dimension generalization of these laws can be written as:

$$\text{for } k \in \{1,\dots,d\}: \begin{cases} {}_{n+1}I^{2k-1}_{(j_1,\dots,j_d)} = {}_nS^{2k}_{(j_1-\delta_{k1},\dots,j_d-\delta_{kd})} \\ {}_{n+1}I^{2k}_{(j_1,\dots,j_d)} = {}_nS^{2k-1}_{(j_1+\delta_{k1},\dots,j_d+\delta_{kd})}, \end{cases} \tag{4}$$

δ being used here as the Kronecker delta. A 2D example of these laws is illustrated by Fig. 2.

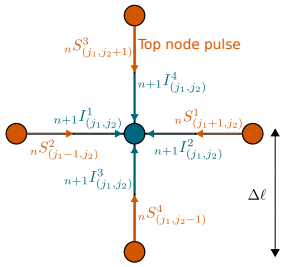

Figure 2: Representation of the 2D connection laws at the local node $\vec{r} = (j_1,\ j_2)$. Scattered pulses "S" (orange) at time step n become incident pulses "I" (blue) at step $n+1$.

Eqs. (1) to (4) are essentials to describing and implementing the TLM model. The link between them and the wave equation will be demonstrated in order to legitimize the resolution method. To do so, a general version of Eq. (1) for each

line is needed; it can be expressed as:

$$ {}_nS^m_{\mathbf{r}} = {}_nR^m_{\mathbf{r}}\,{}_nI^m_{\mathbf{r}} + \sum_{m=1}^{M} {}_nT^m_{\mathbf{r}}\,{}_nI^m_{\mathbf{r}} - T^m_{\mathbf{r}}\,{}_nI^m_{\mathbf{r}},\ m \in \{1,\dots,M\}. \tag{5} $$

Introducing the discrete pressure at the nodes ${}_nP_{\mathbf{r}} = \sum_{m=1}^{M} T^m_{\mathbf{r}}\,{}_nI^m_{\mathbf{r}}$ leads to:

$$ {}_n\,S^m_{\mathbf{r}} = {}_nP_{\mathbf{r}} - {}_nI^m_{\mathbf{r}},\ \forall m\ \in \{1,\dots,M\}. \tag{6} $$

The following sections detail the numerical scheme in the cases of a homogeneous and an inhomogeneous medium and show that Eq. (6) and the discrete pressure expression are valid for both.

3. Scheme for homogeneous non-dissipative media

In this case, the number of transmission lines $m \in \{1,\dots,M = 2\times d\}$, as two nodes are linked to the local node in each spatial direction. Thanks to an electro-acoustical analogy [20] illustrated on Fig. 3, the reflection and transmission coefficients of the pressure at each node can be expressed by inserting $Z^m_{L_{\mathbf{r}}} = Z$ and $Z^m_{T_{\mathbf{r}}} = \dfrac{Z}{2d-1}$ in Eq. (3):

$$ R^m_{\mathbf{r}} = \frac{1-d}{d}, \tag{7a} $$

$$ T^m_{\mathbf{r}} = \frac{1}{d}. \tag{7b} $$

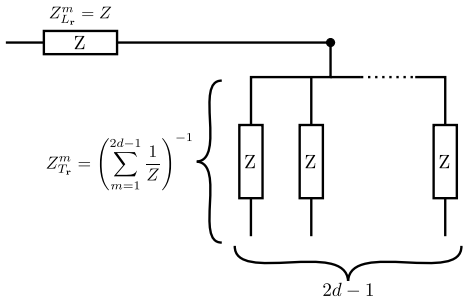

Figure 3: Electrical analogy scheme along one transmission line in the case of a homogeneous non-dissipative medium.

3.1. Link with the wave equation

Using the Millman's theorem [10], the discrete pressure can be expressed as:

$$ {}_nP_{\mathbf{r}} = \frac{1}{d}\sum_{m=1}^{2d} {}_nI_{\mathbf{r}}^{m}. \tag{8} $$

Writing the expression (8) at the the time step $n+1$ and applying twice the Eqs. (4) and (6) leads to [21]:

$$ {}_{n+1}P_{\mathbf{r}} + {}_{n-1}P_{\mathbf{r}} = \frac{1}{d}\sum_{m=1}^{d}\left[{}_nP_{(j_1+\delta_{m1},\ldots,j_d+\delta_{md})} + {}_nP_{(j_1-\delta_{m1},\ldots,j_d-\delta_{md})}\right]. \tag{9} $$

In order to know the approximation order of this scheme, and to retrieve the wave equation, Taylor expansions can be used [12]. It is important to point out that ${}_nP_{(j_1,\ldots,j_d)}$ is an approximated value of the exact pressure $p\left(x_1,\ldots,x_d,t_n\right)$ taken at the point $(x_1,\ldots,x_d)$ at time t_n. Eq. (9) becomes:

$$ \frac{\partial^2 p}{\partial t^2} - c_{\text{TLM}}^2\nabla^2 p = \mathcal{O}\left(\Delta t^2\right) + \mathcal{O}\left(\frac{\Delta\ell^4}{\Delta t^2}\right), \tag{10} $$

with $c_{\text{TLM}} = \dfrac{\Delta\ell}{\sqrt{d}\Delta t}$. It is now possible to recognize the wave equation and to observe that the TLM model is a second-order approximation method in time, and space. Another interesting observation is that the TLM solves the wave equation only if the condition $c_{\text{TLM}}^2 = c_0^2$ is fulfilled. Developing this condition gives:

$$ \frac{c_0\Delta t}{\Delta\ell} = \frac{1}{\sqrt{d}}, \tag{11} $$

which corresponds with the CFL criterion of the so-called finite difference Leap-Frog scheme [6].

3.2. Stability analysis

To evaluate the model stability, the numerical dispersion relation of the method can be written by inserting the formulation of a discretized plane wave ${}_nP_{\mathbf{r}} = A\exp\left(i\left[\sum_{l=1}^{d} k_l j_l\Delta\ell - \omega n\Delta t\right]\right)$ in Eq. (9). Namely:

$$ \cos(\omega\Delta t) = \frac{1}{d}\sum_{m=1}^{d}\cos(k_m\Delta\ell), \quad \forall\Delta t,\ \forall\Delta\ell. \tag{12} $$

This equation implies that the TLM method is unconditionally stable in the homogeneous non-dissipative case. However, this relation also shows that the model presents numerical dispersion in the main directions of the grid (for instance in the 2D case $\theta = \beta\dfrac{\pi}{2},\ \beta\in\mathbb{Z}$). To illustrate this phenomenon, the dispersion error is represented as a function of the angle θ between the plane

wave vector and the horizontal direction of the mesh. Fig. 4 displays three different cases of spatial grid discretizations that are defined as the numbers of nodes per wavelength along the Cartesian directions. These plots show that the relative dispersion error is below 5% when the number of points per wavelength N is greater than 5.

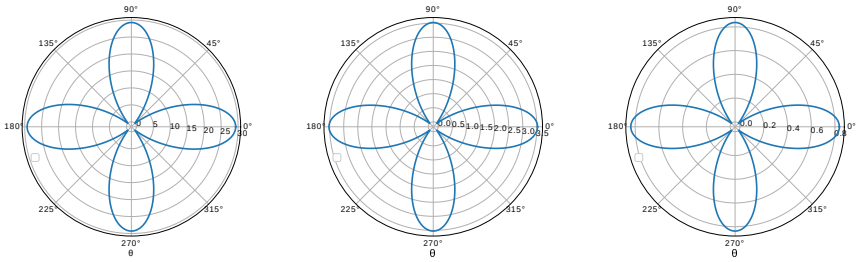

(a) N=2 (b) N=5 (c) N=10

Figure 4: Relative errors on the phase speed [%] related to the model anisotropy depending on the number N: (a) N=2, (b) N=5 and (c) N=10.

4. Scheme for inhomogeneous dissipative media

In order to adapt the model to realistic outdoor scenarios, the inhomogeneous sound velocity and the atmospheric attenuation are modeled by adding two specific transmission lines [14, 19]. Their impedance can vary in both space and time thanks to additional parameters η and ζ defined later in the text (see subsection 4.2 to subsection 4.4). A 2D example of the environment around one node is exposed on Fig. 5. The main differences with the homogeneous and non-dissipative medium case (section 3) lie in the reflection and transmission coefficients in the diffusion matrix ${}_n\underline{\underline{D}}_{\mathbf{r}}$ and the introduction of an additional connection law that are successively detailled in the three following paragraphs.

4.1. Scheme along a regular line

The lines whose superscripts $m \in \{1, \ldots, 2d\}$ behave identically as those presented in section 3. Their impedance depends only on the medium to model.

However, as exposed on Fig. 6, the appearance of two additional lines changes the equivalent impedance encountered by the pulses at the corresponding nodes and leads to the two following expressions of the diffusion matrix coefficients:

$$ {}_nR^m_{\mathbf{r}} = -\frac{{}_n\eta_{\mathbf{r}} + {}_n\zeta_{\mathbf{r}} + 2\,(d-1)}{{}_n\eta_{\mathbf{r}} + {}_n\zeta_{\mathbf{r}} + 2d}, \tag{13a} $$

$$ {}_nT^m_{\mathbf{r}} = \frac{2}{{}_n\eta_{\mathbf{r}} + {}_n\zeta_{\mathbf{r}} + 2d}. \tag{13b} $$

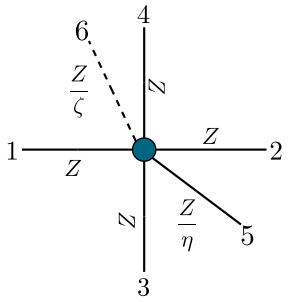

Figure 5: Node transmission lines 2D environment example for an inhomogeneous and dissipative medium.

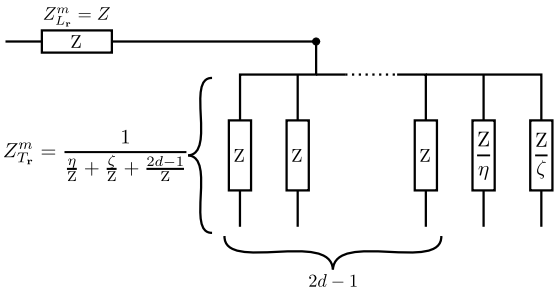

Figure 6: Electrical analogy scheme along regular transmission lines in the case of an inhomogeneous dissipative medium.

4.2. Scheme along a modified impedance line

In order to model local heterogeneity in the sound propagation velocity such as induced by wind or temperature vertical gradients, a transmission line with a reflective termination of length $\frac{\Delta\ell}{2}$ and with superscript $m = 2d+1$, is introduced. The impedance of this branch is set as $Z^{2d+1}_{\mathbf{r}} = \frac{Z}{\eta}$, with η a parameter related to the local effective velocity [19]. As illustrated on Fig. 5, this line is not linked to any other node and is introduced to simulate a volume variation at the node leading to the following modified expressions of the diffusion matrix coefficients [14]:

$$ {}_nR^{2d+1}_{\mathbf{r}} = -\frac{{}_n\eta_{\mathbf{r}} - {}_n\zeta_{\mathbf{r}} - 2d}{{}_n\eta_{\mathbf{r}} + {}_n\zeta_{\mathbf{r}} + 2d}, \tag{14a} $$

$$ {}_nT^{2d+1}_{\mathbf{r}} = \frac{2 \times {}_n\eta_{\mathbf{r}}}{{}_n\eta_{\mathbf{r}} + {}_n\zeta_{\mathbf{r}} + 2d}. \tag{14b} $$

This extra branch at the node implies an additional connection law to the homogeneous and non-dissipative medium case (Eq. (4)) that differs slightly

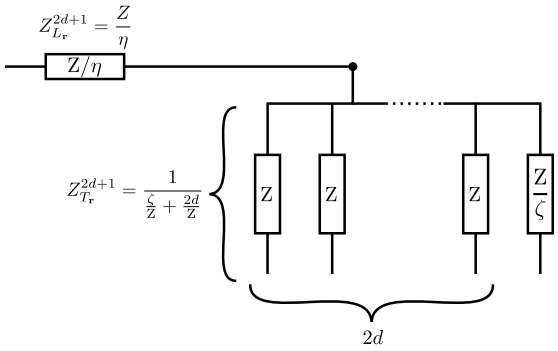

Figure 7: Electrical analogy scheme along the transmission line $2d + 1$ in the case of an inhomogeneous dissipative medium.

from the usual ones since the scattered pulses are reflected back to the node of origin of the pulse, *i.e*:

$$ {}_{n+1}I_{\mathbf{r}}^{2d+1} = {}_{n}S_{\mathbf{r}}^{2d+1}. \tag{15}$$

4.3. Scheme along an anechoic transmission line

One method to include atmospheric absorption in the TLM model without increasing significantly computational costs consists in inserting an anechoic branch of superscript $m = 2d + 2$ and impedance $Z_{\mathbf{r}}^{2d+2} = \dfrac{Z}{\zeta}$ [12]. The parameter ζ is calculated from the atmospheric absorption coefficient α [m^{-1}]. It must be pointed out that, as the α coefficient, the ζ parameter is frequency-dependent. This is the first limitation of this method because it assumes a constant absorption coefficient for the frequency range of the simulation.

There is no reflection nor transmission on this line because its purpose is to simulate an amplitude loss of the wave. It is then straightforward to express the reflection and the transmission coefficients as:

$$ {}_{n}R_{\mathbf{r}}^{2d+2} = {}_{n}T_{\mathbf{r}}^{2d+2} = 0. \tag{16}$$

4.4. Link with the wave equation

Thanks to the previous developments, the coefficients of the $M \times M$ ($M = 2d + 1$) matrix equation are set (Eq. (1)). As done in the homogeneous and non-dissipative case, the discrete nodal pressure is expressed on the basis of

Millman's theorem [10]:

$$ {}_n p_{\mathbf{r}} = \frac{2}{2d+\eta+\zeta}\left(\sum_{m=1}^{2d} {}_n I_{\mathbf{r}}^m + \eta_n I_{\mathbf{r}}^{2d+1}\right), \tag{17a} $$

$$ {}_n p_{\mathbf{r}} = \sum_{m=1}^{2d} {}_n T_{\mathbf{r}}^m {}_n I_{\mathbf{r}}^m + {}_n T_{\mathbf{r}}^{2d+1} {}_n I_{\mathbf{r}}^{2d+1} = \sum_{m=1}^{2d+1} {}_n T_{\mathbf{r}}^m {}_n I_{\mathbf{r}}^m. \tag{17b} $$

For this demonstration, the vertical velocity gradient and the atmospheric absorption loss are considered as time-independent. Thus, the derivation of the equivalent wave equation starts by writing Eq. (17a) at the time step $n+1$:

$$ \frac{2d+\eta+\zeta}{2} {}_{n+1} p_{\mathbf{r}} = \sum_{m=1}^{2d} {}_{n+1} I_{\mathbf{r}}^m + \eta \times {}_{n+1} I_{\mathbf{r}}^{2d+1}. \tag{18} $$

Applying twice the Eqs. (4) and (6) leads to the pressure scheme:

$$ \frac{2d+\eta+\zeta}{2} {}_{n+1} p_{\mathbf{r}} + \frac{2d+\eta-\zeta}{2} {}_{n-1} p_{\mathbf{r}} = $$
$$ \sum_{m=1}^{d} \left[{}_n P_{(j_1+\delta_{m1},\ldots,j_d+\delta_{md})} + {}_n P_{(j_1-\delta_{m1},\ldots,j_d-\delta_{md})} \right] + \eta_n P_{\mathbf{r}}. \tag{19} $$

Finally, using Taylor expansions (as before for the homogeneous case), the terms multiplied by ζ complete the scheme presented in section 3. They approximate the first-order derivative of the pressure and the equivalent wave equation solved by the TLM model in a dissipative inhomogeneous medium is then:

$$ \frac{1}{c_{\mathrm{TLM}}^2}\frac{\partial^2 p}{\partial t^2} - \nabla^2 p + \frac{\zeta_{(j,l)}}{2\Delta\ell^2}\left(2\Delta t \frac{\partial p}{\partial t}\right) = \mathcal{O}\left(\frac{\Delta t^4}{\Delta\ell^2}\right) + \mathcal{O}\left(\frac{\Delta t^3}{\Delta\ell^2}\right) + \mathcal{O}\left(\Delta\ell^2\right), \tag{20} $$

with
$$ c_{\mathrm{TLM}}\left(\mathbf{x}_{\mathbf{r}}\right) = \sqrt{\frac{2}{\eta_{\mathbf{r}}+2d}}\frac{\Delta\ell}{\Delta t}. \tag{21} $$

The meteorological effects are therefore modelled by defining an effective velocity c_{eff} given by [5]:

$$ c_{\mathrm{eff}} = \sqrt{\gamma R T} + \underline{w}.\underline{u}, \tag{22} $$

with γ the heat capacity ratio, R the gas constant, T the temperature in Kelvin, $\underline{w}$ the horizontal wind vector and $\underline{u}$ the unit vector of the direction of sound propagation. Since the condition $c_{\mathrm{TLM}} = c_{\mathrm{eff}}$ must be fulfilled to model the acoustic wave equation, the parameter η is expressed as:

$$ \eta_{\mathbf{r}} = \frac{2\Delta\ell^2}{\Delta t^2\left(\sqrt{\gamma R T} + \underline{w}.\underline{u}\right)^2} - 2d. \tag{23} $$

4.5. Stability analysis

The introduction of a plane wave solution of the form

$$P = P_0 \exp\left(i\left[\sum_{l=1}^{d} k_l x_l - \omega t\right]\right)$$

in Eq. (20) allows to express the norm of the wave vector $\underline{k} = [k_1, \ldots, k_d]^T$ as:

$$\|\underline{k}\|^2 = \frac{\omega^2}{c_{\mathrm{TLM}}^2}\left(1 + i\frac{2\zeta}{(\eta + 2d)\omega\Delta t}\right),$$

which can be reformulated using a first order Taylor expansion:

$$\|\underline{k}\| \approx k_{0\mathrm{TLM}} + i\alpha_{\mathrm{TLM}} + \mathcal{O}(\zeta^2), \tag{24}$$

with $k_{0\mathrm{TLM}} = \dfrac{\omega}{c_{\mathrm{TLM}}}$ the norm of the wave vector in the non-dissipative case and $\alpha_{\mathrm{TLM}} = \dfrac{\zeta}{\sqrt{2(\eta + 2d)}\Delta\ell}$.

Out of these results, it can be observed that the solution of Eq. (20) is an attenuated wave because its amplitude decrease with the distance. However, the dependence of the absorption coefficient α_{TLM} on the parameter η shows that there is a coupling between the heterogeneity model and the absorption. This effect is critical for the validity of the model because the atmospheric absorption effect modeled by the TLM method will be affected by the wind conditions, which should not be the case.

Furthermore, as mentioned in [22], the theoretical absorption coefficient α is frequency-dependent whereas α_{TLM} is not. Hence, this modeling technique of the atmospheric absorption is not suitable for broadband sound prediction in outdoor environments. However, post-filtering the numerical results in order to artificially apply the atmospheric absorption is still possible to compensate this missing feature in the TLM model. If only the heterogeneity of the sound velocity is considered (*i.e* $\zeta = 0$), the insertion of a discretized plane wave in Eq. (19) leads to the dispersion equation:

$$\omega = \frac{1}{\Delta t}\arccos\left(\frac{2\sum_{m=1}^{d}\cos(k_m\Delta\ell) + \eta_{\mathbf{r}}}{\eta_{\mathbf{r}} + 2d}\right). \tag{25}$$

According to Eq. (25) the condition for the scheme to be stable is that the argument of the arccosinus $\in [-1, 1]$, which is met only if $\eta \geq 0$ because the solution $\eta \leq -2d$ is unacceptable. The presence of the $\eta_{\mathbf{r}}$ coefficient in Eq. (25) also shows that the scheme is dispersive. In order to characterize this dispersion, it is necessary to estimate the range of values taken by $\eta_{\mathbf{r}}$.

For a given simulation with valid results until a maximal frequency $f_{\max}$, the spatial discretization should be taken as: $\Delta\ell = \frac{\lambda_{\min}}{N} = \frac{c_{\min}}{f_{\max}N}$, with $c_{\min}$ the minimal sound velocity in the propagation medium. Then, in order to satisfy the stability condition:

$$\frac{\Delta\ell}{\sqrt{d}c_{\text{eff}}} \geq \Delta t,$$

and
$$\Delta t = \frac{\Delta\ell}{\sqrt{d}c_{\max}}, \tag{26}$$

taking $c_{\max}$ as the maximal sound velocity in the propagation medium to respect the stability condition in the worst case.

As in Ref. [19], linear vertical gradients of temperature ($\partial T/\partial z = \pm\, 0,35$ C^o.m^{-1}) and wind speed ($\partial w/\partial z = \pm\, 0,2$ s^{-1}) are assumed. Here the altitude z=0 is just an artifact to set $T(z{=}0) = 20$ C^o and $w(z{=}0) = 0$ m.s^{-1}, there is no ground effect considered in the stability analysis. More realistic profiles, such as linear-logarithmic (called generally "lin-log") vertical velocity profiles, could be used but, given the number of points considered, they would not make a significant difference in the results [5]. Then, the values of η are calculated for downward (*i.e* downwind with a positive temperature vertical gradient) and upward refraction conditions (*i.e* upwind with a negative temperature vertical gradient). These examples are the worst case scenarios since they present the widest ranges of values for c_{eff}. These situations give that $\eta \in [0; 4.82 \times 10^{-1}]$ for downward atmospherical conditions and $\eta \in [0; 5.22 \times 10^{-1}]$ for upward atmospherical conditions.

Figs. 8 and 9 show that the dispersion error is maximal when η is maximal (*i.e* $c_{\text{TLM}} = \min\left(c_{\text{eff}}(z)\right),\ z \in [z_{\min}, z_{\max}]$). The main difference with the homogeneous case is that, for $\theta = \frac{\pi}{4} + \beta\frac{\pi}{2}$ ($\beta \in \mathbb{Z}$), the scheme presents a dispersion error ($\approx 0,4\%$ for $N = 5$). However, theses plots also highlight that this formulation of the TLM model for inhomogeneous media leads to a maximal dispersion error at the bottom part of the grid in the downward case and at the upper part of the grid in the upward case. For long range sound propagation simulation, it is important to keep in mind these limitations of the TLM model. Table 1 displays the minimum and maximum relative dispersion errors for the downward case, which correspond to the errors in the diagonal and the axial direction of the mesh, respectively. The values show that the local errors are acceptable for N=5 and negligible for N=10 and they are close to those obtained in the upward case. However, these are local errors around a node and it is necessary to study their impact at a larger scale in order to oberve the propagation of the dispersion error. Moreover, it is known that dispersion affects the group speed more than the phase speed [23], so the following section aims to analyze its effects on this quantity through a numerical long-range propagation experiment.

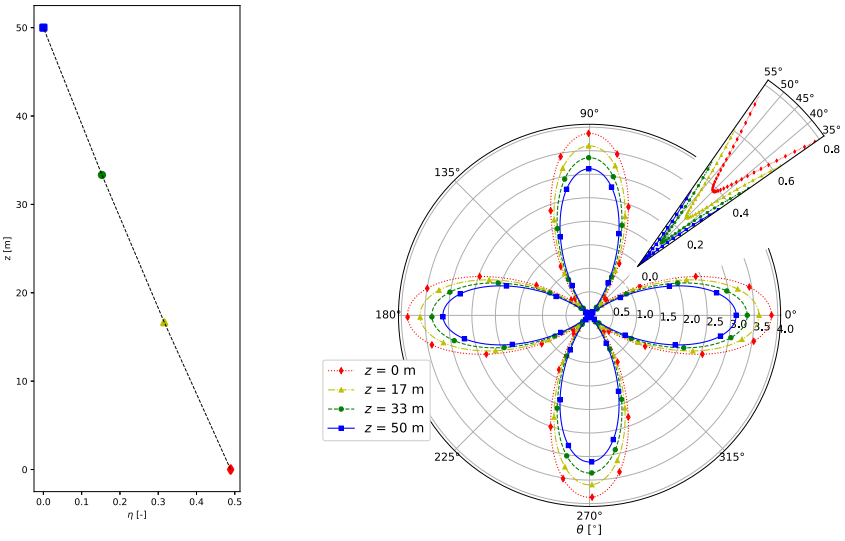

(a) (b)

Figure 8: Modeling of downward refraction conditions for $N = 5$: (a) evolution of η according to the height z; (b) relative errors on the phase speed [%] according to z and θ.

N / η	2		5		10	
	min [%]	max [%]	min [%]	max [%]	min [%]	max [%]
4.89e-01	3.85e+00	3.03e+01	3.85e-01	3.87e+00	9.12e-02	9.26e-01
3.16e-01	2.52e+00	2.86e+01	2.49e-01	3.60e+00	5.89e-02	8.61e-01
1.53e-01	1.24e+00	2.70e+01	1.21e-01	3.35e+00	2.85e-02	8.01e-01
0.00e+00	1.56e-04	2.55e+01	1.74e-05	3.12e+00	4.18e-06	7.44e-01

Table 1: Minimum and maximum values of the relative error on phase speed for various (η, N) configurations, downward case.

5. Numerical experiment

To analyze and quantify the effects of the dispersion highlighted theoretically in sections 3 and 4, a numerical experiment is carried out. Indeed, determining the limits of the TLM predictions at high frequencies according to the distance from a sound source is critical when considering long range sound propagation. The evaluation of these limits would enable the characterization of a critical distance (source-receiver) for a given number of points per wavelength at the maximal frequency. It will set the range at which the dispersion error on the

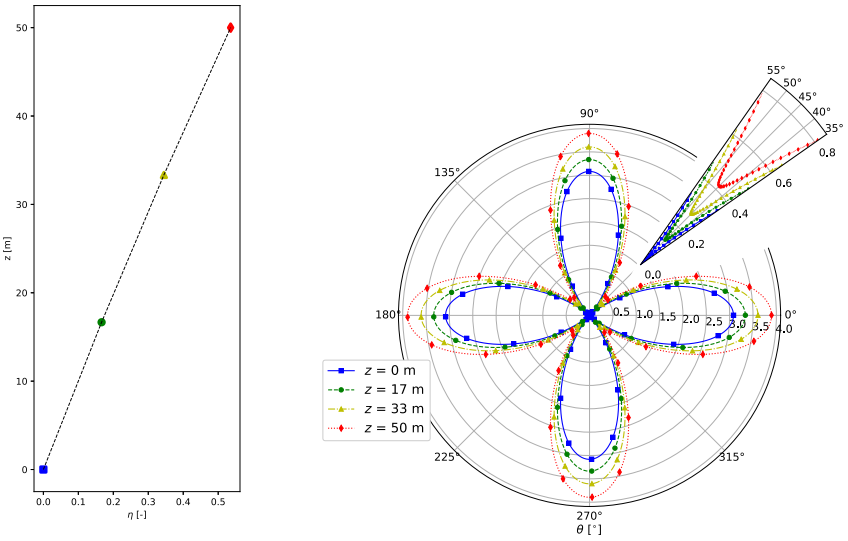

(a) (b)

Figure 9: Modeling of upward refraction conditions for $N = 5$: (a) evolution of η according to the height z; (b) relative errors on the phase speed [%] according to z and θ.

results is too high to consider them relevant.

5.1. Simulation setup

As highlighted through Figs. 4, 8 and 9, a 2D-cartesian mesh implies a higher dispersion error on the axial direction than along the diagonal direction. To analyze this effect in terms of sound pressure level predictions, the setup illustrated in Fig. 10 is simulated. It is composed of a unique sound source surrounded by two arrays of eleven receivers located along the horizontal and diagonal ($\theta = \frac{\pi}{4}$) directions of the mesh.

Long-distance propagation becomes challenging when the frequency reaches high values. The specifications of a configuration used in the following results is given by Table 2 to get an overview of the computing ressources needed. To process the approximately 2700 million points to be solved and support the associated memory load, the TLM model was developed in OpenCL programming language to allow the parallelization of calculations on graphics processing units (GPUs), the parameterization of the simulations being managed on the basis of Python scripts [17]. In the case of the example, the implementation avoids the storage of a 10 Gb matrix and allows to perform the simulation in around 3 hours using three Nvidia GeForce cards GTX 1080 Ti.

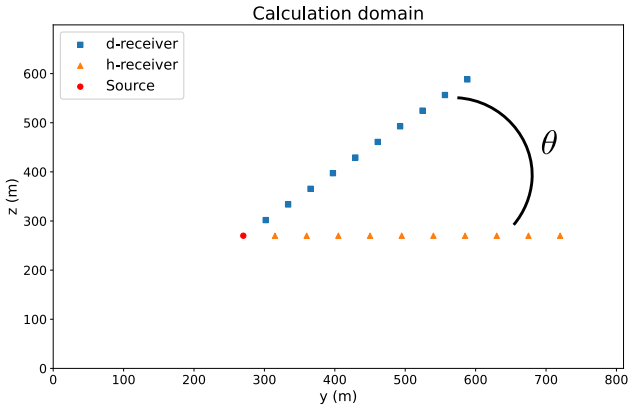

Figure 10: Dispersion analysis setup: the source in the center and microphones are positioned along the horizontal and diagonal ($\theta = \frac{\pi}{4}$) directions.

$\Delta\ell$ [m]	Δt[s]	$\Delta\ell_{\text{mic}}$[m]	$N_y \times N_z$ [-]	Memory [Gb]	t_{comp}[s]	$r_{\max}/\lambda_{\min}$ [-]
1.43e-02	2.95e-05	45	56476 × 48746	10.22	11143	3176

Table 2: Configuration example for a setup with $f_{\max} = 2400$ Hz, $N = 10$, $r_{\max} = 450$ m. $N_y \times N_z$ are the number of integration points in the respective axes. The memory usage is given for a float32 numpy array. t_{comp} is the computation time needed for this configuration.

Note that a comparison of the computational costs of the TLM model with those of more common methods is not straightforward. Indeed, even though the TLM is equivalent to a 2-point FDTD scheme in space and time, its implementation is not based on an explicit scheme of the form $P^{n+1} = f(P^n)$. The decomposition into $2 \times d$ pulses at each point allows the calculations to be divided into parallelizable computational subdomains as described in [17]. This method significantly reduces the computation time but multiplies by $2 \times d$ the memory usage.

5.2. Sound source

The omnidirectional point source used in this experiment is a time-dependent Gaussian pulse, namely:

$$S(\underline{r}_s, n) = \exp\left(-\pi^2 \left(f_c n \Delta t - 1\right)^2\right), \tag{27}$$

with a parameter $f_c = f_{\max}/2$ which guarantees that the frequency support of the source reaches the maximal frequency $f_{\max}$.

5.3. Analytical solution

The simulation results are compared with the analytical solution in free-field for a monopole source [24], defined as a spherical source with a Gaussian mass

flow [25]:

$$q(\underline{r},t) = 4\pi\epsilon^2 v(\underline{r} = \underline{r}_0 + \underline{\epsilon}) \exp(-\pi^2(f_c t - 1)^2)\delta(\underline{r} - \underline{r}_0)\mathrm{H}(t) = Q_0(t)\delta(\underline{r} - \underline{r}_0), \tag{28}$$

$\mathrm{H}(t)$ being the Heaviside function and $\delta(\underline{r} - \underline{r}_0)$ the spatial Dirac density such that $\int_\Omega \delta(\underline{r} - \underline{r}_0)d\Omega = 1$. Applying the Fourier transform to the sound wave equation leads to the Helmoltz equation:

$$\Delta\hat{h}(\underline{r},\omega) + k_w^2\hat{h}(\underline{r},\omega) = -\delta(\underline{r} - \underline{r}_s), \tag{29}$$

with $\hat{h}(\underline{r},\omega) = \dfrac{\hat{P}(\underline{r},\omega)}{-i\omega\rho_0\hat{Q}_0(w)}$ and $k_w = \pm\dfrac{w}{c}$.

The known solutions of this equation in free-field are the following Green functions:

$$\hat{G}_d(\underline{r},\omega) = \begin{cases} \frac{1}{4i}H_0^{(1)}(-k_w r) \text{ in 2D, } H_0^{(1)} \text{ being the Hankel function of the first kind;} \\ \\ \frac{\exp(-ik_w r)}{4\pi r} \text{ in 3D.} \end{cases}$$

The acoustic pressure field can finally be expressed in the frequency and time domains respectively by:

$$\hat{P}(\underline{r},\omega) = -i\omega\rho_0\hat{Q}_0(w)\hat{G}_d(\underline{r},\omega) \tag{30}$$

and

$$p(\underline{r},t) = TF^{-1}\left\{-i\omega\rho_0\hat{Q}_0(w)\hat{G}_d(\underline{r},\omega)\right\}. \tag{31}$$

This analytical solution is then considered as a reference to estimate the validity of the model and the errors among the numerically predicted pressure fields.

5.4. Results

This section aims at analyzing the results of the numerical experiment with a broadband sound source ($f_{\max} = 2400$ Hz) comparing the case $N = 10$ and $N = 5$ points per wavelength. In Fig. 11, the envelope pressure of the signal at the receivers is displayed according to the reduced time $(t_n - \dfrac{r}{c_0})$ which allow an observation of the flattening of the signal along the propagation distance. The effect of the dispersion along the horizontal array of microphones is directly noticeable: the results displayed on Fig. 11 show an apparent decrease of the group speed while the propagation distance increases. For a better visualisation of this delay, the vertical lines on Fig. 11 indicate the moment when 95 % of the signal energy has reached the microphone. Only the $N = 10$ case is shown below because a coarser grid brings longer delays but the overall behavior of the pressure envelopes is equivalent.

This phenomenon is confirmed by the Figs. 12(a) and 12(c) which shows a maximal relative error of 0.7% and 2.9% compared to the analytical solution

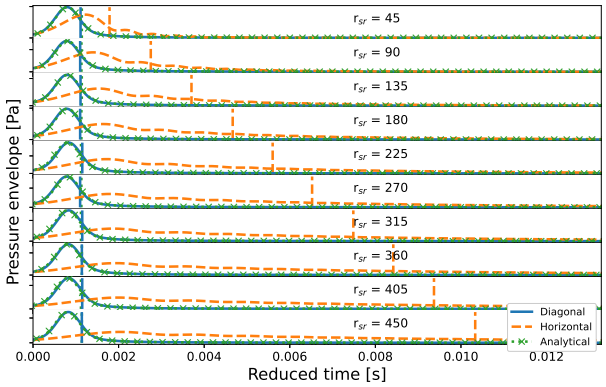

Figure 11: Normalized pressure envelopes at the microphones as dependent upon reduced time, for N=10 grid points per wavelength. Vertical lines indicates the arrival of 95 % of the signal energy.

on the horizontal array of microphones. However, even if the group speed is impacted, the Figs. 12(b) and 12(d) shows that the calculated equivalent sound pressure levels (Leqs) are close to the analytical solution which confirms that the TLM is a dispersive numerical method but not a dissipative one. The simulated Leqs are therefore not affected in free-field because they are calculated with windowed integrals, which integrate the whole signal energy.

To better understand the frequency behavior of the dispersion, a one-third octave band decomposition has been performed on the microphones signals and the relative group speed error has been calculated for each band. The results of this post-processing are displayed on Figs. 13 and 14 and they imply that the high frequency contents are more delayed compared to the analytical solution and to the results from the diagonal array. The difference between the $N = 5$ and the $N = 10$ case is significant and shows that the impact of the number of points per wavelength on the error is prevailing on the propagation of the error along the source-receiver distance.

These plots highlight that the inherent dispersion of the TLM model is impacting free-field long distance simulation results. Even if the impact is below 2% compared to the analytical solution at 450 m and $N = 10$ for 2400 Hz, further investigation is needed to characterize the effect of dispersion when a ground reflection is simulated. Indeed, if the high frequency components of the signal are delayed, interfence patterns may occur between the direct field pulse and the reflected signal and consequently impact the energy of the signal received at the microphones. In this case, the TLM dispersion could impact the simulated sound pressure levels which is critical in the field of sound propagation predictions in the outdoor environment.

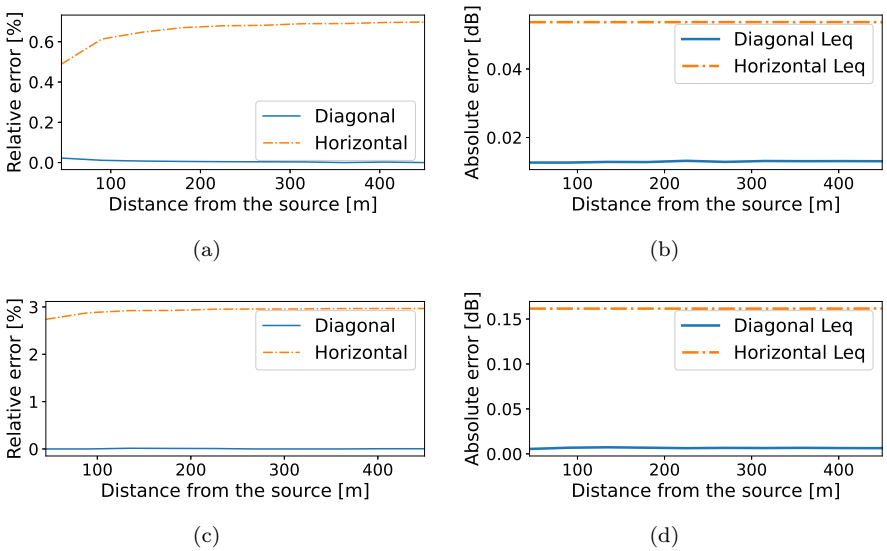

Figure 12: Comparison between the signals received at the microphones and the analytical solution depending on the propagation distance (a) & (c) magnitude of the errors on the group velocities for $N = 10$ and $N = 5$ respectively; (b) & (d) absolute errors on Leqs for $N = 10$ and $N = 5$ respectively.

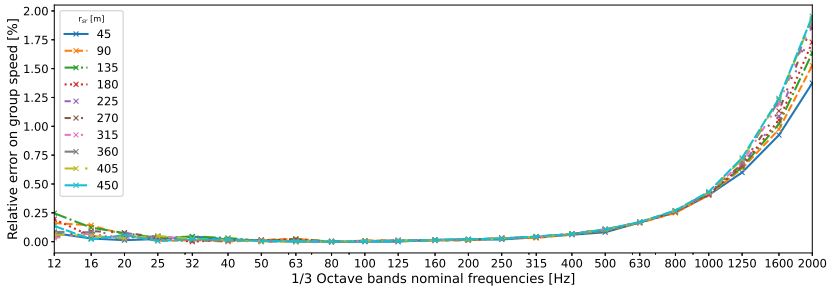

Figure 13: group speed error plots depending on the one-third octave band decomposed frequencies and the distance to the source for $N = 10$ for the horizontal array.

6. Conclusion

The usage of the TLM model as a solver for long-range outdoor sound propagation was discussed through both theoretical and numerical aspects. The general formulation of the method was renewed and a proper way of linking it to the wave equation was proposed. Thanks to these developments, the inherent anisotropic dispersion of the model has been highlighted in two different cases and the non-validity of the usual atmospheric absorption has been pointed out.

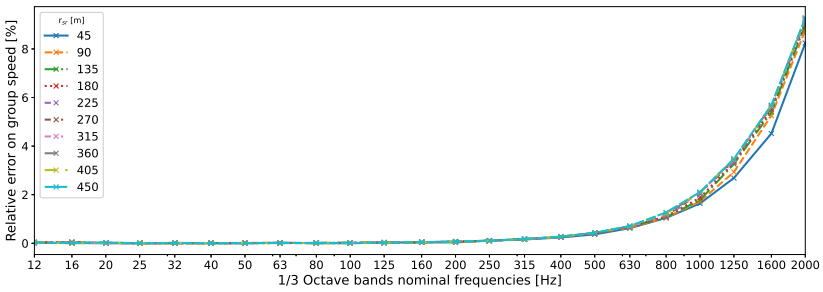

Figure 14: group speed error plots depending on the one-third octave band decomposed frequencies and the distance to the source for $N = 5$ for the horizontal array.

Finally, a numerical experiment has been set to characterize the effects of the dispersion on long-range free-field outdoor propagation results. From the results of this experiment and the theoretical study, the conclusion that the TLM results are valid in this configuration can be drawn provided that the number of point per wavelength is chosen wisely. Indeed, if N is too high, it will lead to significant computational costs and if N is too low, the dispersion error will reduce the frequency range of validity of the results compared to the maximal simulated frequency. However, the observed effects on the group speed of the test signals in the main mesh directions must be taken into account when using the TLM. In the case of predictions for sound propagation in outdoor environments, equivalent sound pressure levels are the primary quantity of interest for the evaluation of sound disturbances. For now, the importance of TLM dispersion in presence of boundary conditions such as natural ground is unknown. Thus, future work needs to be done regarding TLM for modeling realistic long-range sound fields.

Acknowledgments

The authors would like to acknowledge the High Performance Computing Center of the University of Strasbourg for supporting this work by providing scientific support and access to computing resources. Part of the computing resources were funded by the Equipex Equip@Meso project (Programme Investissements d'Avenir) and the CPER Alsacalcul/Big Data.

Appendix A. Relative errors on phase speed for $N = 10$

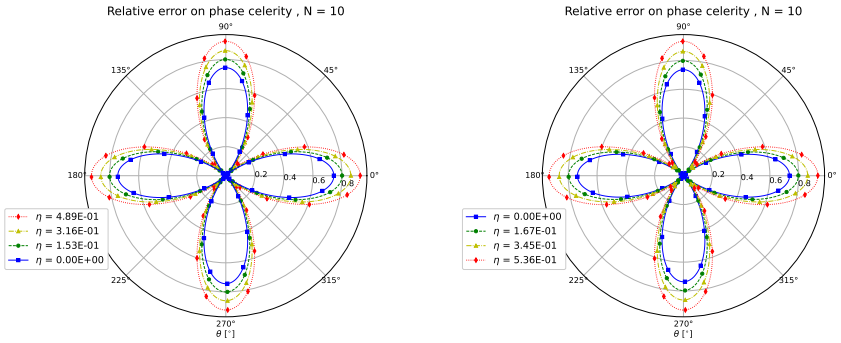

(a) (b)

Figure A.15: Relative errors on the phase speed [%] according to η and θ for N=10: (a) downward conditions; (b) upward conditions.

References

[1] F. Theakston, Weltgesundheitsorganisation (Eds.), Burden of Disease from Environmental Noise: Quantification of Healthy Life Years Lost in Europe, World Health Organization, Regional Office for Europe, Copenhagen, 2011.

[2] P. S. Warren, M. Katti, M. Ermann, A. Brazel, Urban bioacoustics: It's not just noise, Animal Behaviour 71 (3) (2006) 491–502. doi:10.1016/j.anbehav.2005.07.014.

[3] R. Sordello, O. Ratel, F. Flamerie De Lachapelle, C. Leger, A. Dambry, S. Vanpeene, Evidence of the impact of noise pollution on biodiversity: A systematic map, Environmental Evidence 9 (1) (2020) 20. doi:10.1186/s13750-020-00202-y.

[4] M. Hornikx, Ten questions concerning computational urban acoustics, Building and Environment 106 (2016) 409–421. doi:10.1016/j.buildenv.2016.06.028.

[5] E. Salomons, Computational Atmospheric Acoustics, Vol. 22, 2001. doi:10.1007/978-94-010-0660-6.

[6] G. C. Cohen, Higher-Order Numerical Methods for Transient Wave Equations, Vol. 110 of Scientific Computation, Springer Berlin Heidelberg, Berlin, Heidelberg, 2002. doi:10.1007/978-3-662-04823-8.

[7] M. Hornikx, openPSTD: The open source pseudospectral time-domain method for acoustic propagation, Computer Physics Communications 203 (Jun. 2016). doi:10.1016/j.cpc.2016.02.029.

[8] P. Johns, R. Beurle, Numerical solution of 2-dimensional scattering problems using a transmission-line matrix, Proceedings of the Institution of Electrical Engineers 118 (9) (1971) 1203–1203. doi:10.1049/piee.1971.0217.

[9] P. Johns, On the Relationship Between TLM and Finite-Difference Methods for Maxwell's Equations (Short Paper), IEEE Transactions on Microwave Theory and Techniques 35 (1) (1987) 60–61. doi:10.1109/TMTT.1987.1133595.

[10] D. de Cogan, W. J. O'Connor, S. Pulko, Transmission Line Matrix (TLM) in Computational Mechanics, CRC Press, 2005. doi:10.1201/9780203022184.

[11] G. Guillaume, J. Picaut, G. Dutilleux, B. Gauvreau, Time-domain impedance formulation for transmission line matrix modelling of outdoor sound propagation, Journal of Sound and Vibration 330 (26) (2011) 6467–6481. doi:10.1016/j.jsv.2011.08.004.

[12] Y. Kagawa, T. Tsuchiya, B. Fujii, K. Fujioka, Discrete Huygen's model approach to sound wave propagation, Journal of Sound and Vibration 218 (3) (1998) 419–444. doi:10.1006/jsvi.1998.1861.

[13] Y. Kagawa, T. Tsuchiya, K. Fujioka, M. Takeuchi, Discrete Huygens' model approach to sound wave propagation—reverberation in a room, sound source identification and tomography in time reversal, Journal of Sound and Vibration 225 (1) (1999) 61–78. doi:10.1006/jsvi.1999.2227.

[14] Y. Kagawa, T. Tsuchiya, T. Hara, T. Tsuji, Discrete Huygens' modelling simulation of sound wave propagation in velocity varying environments, Journal of Sound and Vibration 246 (3) (2001) 419–439. doi:10.1006/jsvi.2001.3637.

[15] G. Guillaume, J. Picaut, G. Dutilleux, Use of the transmission line matrix method for the sound propagation modeling in urban area, The Journal of the Acoustical Society of America 123 (5) (2008) 3924–3924. doi:10.1121/1.2935958.

[16] P. Chobeau, G. Guillaume, J. Picaut, D. Ecotière, G. Dutilleux, A Transmission Line Matrix model for sound propagation in arrays of cylinders normal to an impedance plane, Journal of Sound and Vibration 389 (2017) 454–467. doi:10.1016/j.jsv.2016.11.005.

[17] G. Guillaume, N. Fortin, Optimized transmission line matrix model implementation for graphics processing units computing in built-up environment, Journal of Building Performance Simulation 7 (6) (2014) 445–456. doi:10.1080/19401493.2013.864335.

[18] P. Aumond, G. Guillaume, B. Gauvreau, C. Lac, V. Masson, M. Bérengier, Application of the Transmission Line Matrix method for outdoor sound propagation modelling – Part 2: Experimental validation using meteorological data derived from the meso-scale model Meso-NH, Applied Acoustics 76 (August 2005) (2014) 107–112. doi:10.1016/j.apacoust.2013.07.015.

[19] G. Guillaume, P. Aumond, B. Gauvreau, G. Dutilleux, Application of the transmission line matrix method for outdoor sound propagation modelling - Part 1: Model presentation and evaluation, Applied Acoustics 76 (2014) 113–118. doi:10.1016/j.apacoust.2013.07.011.

[20] I. J. Scott, D. de Cogan, An improved transmission line matrix model for the 2D ideal wedge benchmark problem, Journal of Sound and Vibration 311 (3-5) (2008) 1213–1227. doi:10.1016/j.jsv.2007.10.009.

[21] J. Hofmann, K. Heutschi, Simulation of outdoor sound propagation with a transmission line matrix method, Applied Acoustics 68 (2) (2007) 158–172. doi:10.1016/j.apacoust.2005.10.006.

[22] T. Tsuchiya, Numerical simulation of sound wave propagation with sound absorption in time domain, 13th International Congress on Sound and Vibration 2006, ICSV 2006 4 (2006) 2839–2846.

[23] L. N. Trefethen, Group Velocity in Finite Difference Schemes, SIAM Review 24 (2,) (1982) 113–136.

[24] W. Duan, R. Kirby, The sound power output of a monopole source in a cylindrical pipe containing area discontinuities, in: Acoustics 2012, Nantes, France, 2012, p. 7.

[25] M. Bruneau, Fundamentals of Acoustics, ISTE Ltd, London ; Newport Beach, CA, 2006.